Current Zoology, 2023, **69**, 475–490
https://doi.org/10.1093/cz/zoac057
Advance access publication 1 August 2022
Original Article

Cranial differences in three-toed jerboas (Dipodinae, Dipodidae, Rodentia) according to recent taxonomic revisions

Bader H. Alhajeri, Zahraa Hasan, and Hasan Alhaddad

Department of Biological Sciences, Kuwait University, Safat, 13060, Kuwait

*Address correspondence to Bader H. Alhajeri. E-mail: bader.alhajeri@ku.edu.kw
Handling editor: Zhi-Yun Jia

Abstract

Recent phylogenetic studies amended the taxonomy of three-toed jerboas (subfamily Dipodinae), including raising subspecies to full species. Here, we use geometric morphometrics to compare scaled-shape differences in dipodine crania while considering their revised taxonomy. We sampled *Dipus deasyi*, *D. sagitta halli*, *D. s. sowerbyi*, *Jaculus blanfordi blanfordi*, *J. hirtipes*, *J. jaculus*, *J. loftusi*, *J. orientalis gerboa*, *J. o. mauritanicus*, and *Stylodipus andrewsi*. Crania were not sexually dimorphic. Common allometry explained some of the shape variation, for example, reduced braincases in larger specimens. Most operational taxonomic unit pairs differed in both size and shape. *Dipus* and *Stylodipus* clustered together based on their cranial shape. *Jaculus* differed from the aforementioned genera by its larger tympanic bulla, broader braincase, larger infraorbital foramen, along with reduced molars and rostra. *Jaculus orientalis* differed from other *Jaculus* by its broader face versus reduced cranial vault. *Jaculus blanfordi* (subgenus *Haltomys*) resembles members of the subgenus *Jaculus* more than its consubgener (*J. orientalis*). *Jaculus loftusi*, previously considered a synonym of *J. jaculus*, clearly differed from the latter by its shorter rostrum, smaller infraorbital foramen, and more caudolaterally expanded tympanic bulla. *Jaculus hirtipes*, another recent synonym of *J. jaculus*, resembled *J. blanfordi* more in scaled cranial shape than it did *J. jaculus*. *Dipus sagitta halli* and *D. s. sowerbyi* were indistinguishable, but they clearly differed from *D. deasyi* (recently raised to full species) with the latter having a larger molar row, more inflated tympanic bulla, and shorter, slenderer rostrum. Ecological explanations for detected cranial shape differences are considered, including diet and habitat (particularly substrate).

Key words: crania, *Dipus deasyi*, *Jaculus hirtipes*, *Jaculus loftusi*, jerboa, *Stylodipus andrewsi*.

Three-toed jerboas (subfamily Dipodinae Fischer, 1817) are named after their tridigitated hindfeet, adapted to leaping. This is accompanied by a long counterbalancing tail, fused metatarsals (firm elongate hindfeet have more load-bearing capacity), and cervical vertebrae (rigid short neck withstands the stress of saltation) (Hutchins et al. 2003; Kingdon et al. 2013). In contrast, forelimbs are diminished and retain all 5 digits, which are mainly used for food handling and burrow excavation, not locomotion (Kingdon et al. 2013). Jerboas are nocturnal, using burrows during the day to hide from their predators, for example, raptors, small carnivorans, and snakes (Shenbrot et al. 2008), and during cold parts of the year to hibernate or for multiday torpor (Michaux and Shenbrot 2017). But jerboa burrows mainly reduce daytime evaporative water loss, being sealed in the summer (Hoath 2003), and are one of many adaptations to aridity. Other such adaptations include efficient kidneys (producing concentrated urine with little water loss) allowing them to live without free water while surviving on a dry food diet, for example, seeds and grass (Kingdon et al. 2013).

Jerboas inhabit sandy, clayey, and gravelly areas of the arid southern Palearctic, with a proclivity for stabilized substrate, for example, clay, in the 5-toed allactagines versus loose sandy soil in dipodines (Hutchins et al. 2003). However, in addition to sand specialists, 3-toed jerboas also include species specialized to clay, as well those that can use varied substrate (Shenbrot et al. 2008). Plantar pads of jerboas adapted to solid soil exhibit prominent conical calluses, improving substrate adherence (Shenbrot et al. 1999), while those of species occurring in loose sand are covered with long tough hair brushes increasing friction (Hutchins et al. 2003). Jerboas' pinnae are large compared to other rodents, but relatively small in dipodines (Michaux and Shenbrot 2017). This is perhaps due to psammophilly, as they are also often covered with a tuft of bristles to keep dust out of the eardrum (Nowak and Paradiso 1983). Three-toed jerboas burrow predominantly using their foreclaws, often also incorporating their teeth when excavating hard substrate—incisors tend to be larger in species clay-occupying species than those occupying sand (Shenbrot et al. 1999). Other cranial structures are also used, for example, *Jaculus* Erxleben, 1777 rostra are used to shovel sand out of burrows, during which nostrils protected by retractable skinfolds, and eyes by enlarged zygomatic plates (Nowak and Paradiso 1983; Kingdon et al. 2013).

A conservative taxonomic view, that is, Holden and Musser (2005), divides subfamily Dipodinae into 9 species and 5 genera. Three of these 5 genera are monotypic: *Dipus* Zimmermann, 1780 with *D. sagitta* Pallas, 1773 (northern 3-toed jerboa), *Eremodipus* Vinogradov, 1930, with *E. lichtensteini* Vinogradov, 1927 (Lichtenstein's jerboa), and *Paradipus* Vinogradov, 1930, with *P. ctenodactylus* Vinogradov, 1929

Received 11 May 2022; accepted 17 July 2022

(comb-toed jerboa). The remaining two genera are (1) *Jaculus*, with *J. blanfordi* Murray, 1884 (Blanford's jerboa), *Jaculus jaculus* Linnaeus, 1758 (lesser Egyptian jerboa), and *J. orientalis* Erxleben, 1777 (greater Egyptian jerboa), along with (2) *Stylodipus* G. M. Allen, 1925, with *S. andrewsi* G. M. Allen, 1925 (Andrews's 3-toed jerboa), *S. sungorus* Sokolov and Shenbrot, 1987 (Mongolian 3-toed jerboa), and *S. telum* Lichtenstein, 1823 (thick-tailed 3-toed jerboa). This subfamily also includes the newly described *Chimaerodipus auratus* Shenbrot et al. (2017). Other species have also been recently described within the abovementioned genera (see below). According to recent molecular phylogenies, for example, Shenbrot et al. (2017), *Paradipus* branches off first, followed by *Dipus*, and then *Stylodipus* + *Chimaerodipus* which are sister to *Jaculus* + *Eremodipus* (all genera are monophyletic) (Figure 1).

Dipodines are highly variable, both at the inter- and the intraspecific levels. Numerous *Jaculus* populations have been identified as subspecies based on morphological characters (e.g. Setzer 1956; Happold 1967; Ranck 1968; Corbet 1978; Osborn and Helmy 1980; Ben Faleh et al. 2010, 2012). The use of population genetics and molecular phylogenetics has led to substantial taxonomic revision of 3-toed jerboas, including the raising of subspecies to full species. For example, the widely distributed lesser Egyptian jerboa is now commonly separated into 3 species based on mitochondrial and nuclear gene sequences. These constitute 2 sympatric mostly North African species *J. jaculus sensu stricto* and the African hammada jerboa *J. hirtipes* Lichtenstein, 1823 (often referred to using the junior synonym *J. deserti* Loche, 1867), and the allopatric Arabian jerboa *J. loftusi* Blanford, 1875, which mostly occupies the

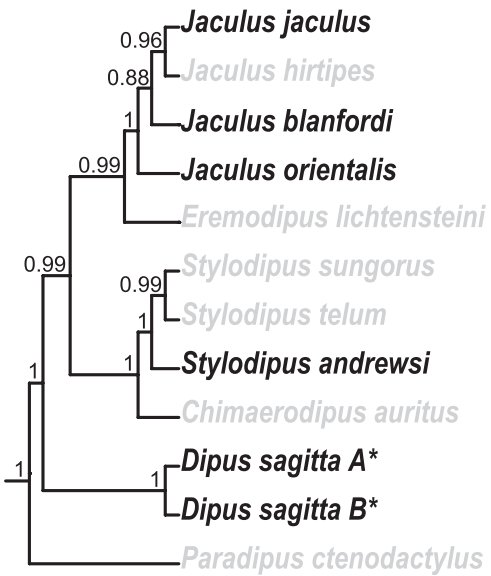

Figure 1. Dipodinae relationships based the molecular phylogeny of Shenbrot et al. (2017). Relationships are simplified as cladograms (with arbitrary branch lengths). The dipodine clade was extracted from a larger phylogeny that includes other dipodids. The Shenbrot et al. (2017) tree used to construct this cladogram is a species tree inferred from 4 nuclear genes and 1 mitochondrial gene, with posterior clade probabilities shown on the respective nodes. The species examined in the present study are indicated in black. The asterisks (*) indicate 2o lineages of *D. sagitta* retrieved by Shenbrot et al. (2017), while we include several subspecies of *D. sagitta*, we do not necessarily sample these two lineages. The cladogram was generated using the R library *ape* (Paradis and Schliep 2019).

Arabian Peninsula (Ben Faleh et al. 2012; Boratyński et al. 2014; Shenbrot et al. 2016). The two sympatric species differ in fur and tail color patterns and male genitalia characters (Shenbrot et al. 2016), and less so in skull morphology (Ben Faleh et al. 2010, 2013) and habitat preference, for example, *J. jaculus* mostly occurs in sandy areas while *J. hirtipes* on rocky substrate (Boratyński et al. 2014). Thaler's jerboa *J. thaleri* Darvish and Hosseinie, 2005 has been described based on 3 specimens from east Iran, being sympatric to and closely related to *J. blanfordi*, from which it differs in karyotype and in missing the usual white flag at the tail tip (Darvish and Hosseini 2005). However, Michaux and Shenbrot (2017) consider this taxon to be just an atypical phenotype of Blanford's jerboa. Two allopatric genetic clades have been identified in *J. orientalis* (Ben Faleh et al. 2016), mostly distributed in accordance to the previously named subspecies *J. o. gerboa* Olivier, 1800 (east Libya to west Egypt) and *J. o. mauritanicus* Duvemoy, 1841 (west Libya to Morocco) (see Michaux and Shenbrot 2017)—a taxonomic revision was conducted by Shenbrot (2013).

The widespread, monospecific northern 3-toed jerboa is another recent focus of taxonomic enquiry. *Dipus sagitta* populations are chromosomally polymorphic and morphologically variable, often divided into ~16 subspecies, and recent genetic evidence suggests that it may hold cryptic species (see Shenbrot et al. 2008; Michaux and Shenbrot 2017). These subspecies are geographically structured (mainly west vs. east) and morphologically distinguishable (particularly the eastern populations) based on fur color "brightness" and skull measurements, for example, overall size, tympanic bulla in particular (see Shenbrot et al. 2008; Lebedev et al. 2018). Based on hindlimb, genital, and karyotypic characters, Shenbrot et al. (2008) place most Central Asian *D. sagitta* populations in the "Sagitta" group and most Russian and Kazakhstan populations in the "lagopus" group. Cheng et al. (2019) found 6 mitochondrial DNA lineages in the "Sagitta" group consistent with some of the previously described subspecies, showing some habitat segregation. Sampling both *D. sagitta* groups, Lebedev et al. (2018) also found mitochondrial lineages corresponding with some subspecies (particularly in the east, some even supported by nuclear data), supporting the idea that the northern 3-toed jerboa is a species complex. One lineage was particularly divergent, which they recognized as *D. deasyi* Barrett-Hamilton, 1900, although they suggested revising its original description (Lebedev et al. 2018). Based on mitochondrial and nuclear genes, Cheng et al. (2018) supported the specific status of *D. deasyi*, which constitutes a phylogenetic group, and detected 3 other such groups.

In this study, we compare the crania of 3-toed jerboas across and within genera. Intrageneric comparisons are at the subspecific or specific level and discussed considering the aforementioned taxonomic revisions. We concentrate on morphologically similar and closely related taxa, especially those that are formerly considered as conspecific, for example, the *J. jaculus* and *Dipus* groups. We use geometric morphometric methods (GMM; see Zelditch et al. 2012) to compare scaled-shape differences, thus gaining insights that may differ from traditional 1-dimensional distance-based approaches, which tend to heavily correlate with size. These methods recently provided taxonomic insights into other rodents (e.g. Beolchini and Corti 2004; Zelditch et al. 2012; Martínez et al. 2016; Tabatabaei Yazdi and Alhajeri 2018; Marr and MacLeod 2019; Li et al. 2020; Alhajeri 2022a). We also explore the extent of intraspecific variation and various ecological explanations for cranial shape differences.

Materials and Methods

Taxonomic sampling

We sampled specimens from the American Museum of Natural History (AMNH) in New York City, the Field Museum of Natural History (FMNH) in Chicago, the Museum of Vertebrate Zoology (MVZ) in the University of California at Berkeley, and the United States National Museum of Natural History (USNM) in Washington DC. Of the 235 specimens that we used, 129 were males, 104 were females, and 2 were unidentified; there were unbiased proportions of either sex in each species.

We did not follow the taxonomy used by the museums, which is mostly concordant with Holden and Musser (2005). Rather, the specimens were recategorized up to the subspecific level following mostly Michaux and Shenbrot (2017) but also based on Ranck (1968), Boratyński et al. (2014), Lebedev et al. (2018), and Cheng et al. (2018). More information about the process of recategorization (along with the original taxonomy of each specimen based on the museum database) can be found in Data S1. We sampled 10 operational taxonomic units (OTUs): *D. deasyi* (N = 1), *D. s. halli* Sowerby, 1920 (N = 18), *D. s. sowerbyi* Thomas, 1908 (N = 14), *J. b. blanfordi* (N = 50), *J. hirtipes* (N = 7), *J. jaculus* (N = 61), *J. loftusi* (N = 2), *J. o. gerboa* (N = 57), *J. o. mauritanicus* (N = 7), and *Stylodipus andrewsi* (N = 18) (Appendix A; Data S1). The specimens identified as *J. jaculus* were split into 2 groups, those from Libya are considered to be *J. jaculus sensu stricto* (N = 34; henceforth referred to as "*J. jaculus*") following Ranck (1968) and Boratyński et al. (2014), while those from Egypt (N = 27; henceforth referred to as "*J. jaculus* Egypt") may include the sympatric *J. hirtipes*—there is no way to know a priori without genetic identification (see Data S1 for more details). Subspecific names were not used in species formerly synonymized with *J. jaculus* as they are problematic and are currently undergoing revision. Our sample excludes specimens with third molars that are incompletely erupted or crania that are considerably damaged.

The specimens spanned 10 countries from Morocco to China and 85 localities (Figure 2; Data S1). Most of the specimens were from Egypt (N = 82) followed by Libya (N = 43) (Data S1). We obtained the specimens' localities (and their geographic coordinates) from the databases of the AMNH (sci-web-001.amnh.org/db/emuwebamnh), the FMNH (collections-zoology.fieldmuseum.org), the MVZ (arctos.database.museum/mvz_mamm), and the USNM (collections.nmnh.si.edu/search/mammals). Georeferencing data were not available in museum databases for 33 localities (77 specimens) (Data S1). We georeferenced these localities using the National Geospatial-Intelligence Agency (NGA) geographic gazetteer (geonames.nga.mil/namesgaz), Google Maps (Google 2020), or MINDAT (mindat.org) (see Data S1 for details). For some localities, we used the distance-measuring tool in Google Maps (Google 2020) for georeferencing as described in previous studies (e.g. Alhajeri 2021a). All geographic coordinates were obtained in decimal degrees. We used the georeferencing data both to assign specimens a subspecific or specific epithet (see above) and to visualize their distribution in a map using the R (R Core Team 2020) libraries *rnaturalearth* (South 2017) and *ggplot2* (Wickham 2016).

Morphometric analysis

We based statistical significance in all analyses on permutation tests—with 999 iterations, a random starting seed, and an α of 0.05 (P-value). Unless otherwise stated, we used base R functions and functions from both the *geomorph* (Adams et al. 2020) and the *RRPP* (Collyer and Adams 2018) libraries to analyze and visualize the data.

We took standardized photographs of the dorsal and the ventral view of each cranium using a D3200 DSLR camera equipped with a 40-mm Micro NIKKOR lens (Nikon, Tokyo, Japan) using the same protocol outlined in previous studies (e.g. Alhajeri 2019). We included 1-mm graph paper next to each cranium before photography to convert pixels to millimeters. We then digitized 26 dorsal and 25 ventral landmarks (Figure 3; Table S1) in the left half of each cranium using ImageJ (Schneider et al. 2012). The chosen landmarks cover biologically important cranial features and are found in most rodents, including allactagine jerboas (see Alhajeri 2021b). Some crania were broken on their left but not their right side; in these cases, we digitally reflected the right view and digitized it instead. We omitted specimens damaged on both sides only in the relevant view (dorsal view N = 224; ventral view N = 226) (Data S1).

We then combined the landmark coordinates into a single tps file (Rohlf 2015) and flipped them to appear right side up in R. Some landmarks could not be digitized in damaged specimens, and thus we estimated their positions using thin-plate spline (TPS; Gunz et al. 2009) using all complete specimens of each genus (separately) as a reference. We then utilized generalized Procrustes analysis (Rohlf and Slice 1990) to superimpose the landmark coordinates and project them onto tangent space—the result was Procrustes shape coordinates and centroid sizes (natural log-transformed in subsequent analyses) (Data S1). We confirmed the absence of large digitization errors by sorting specimens by Procrustes distance from the

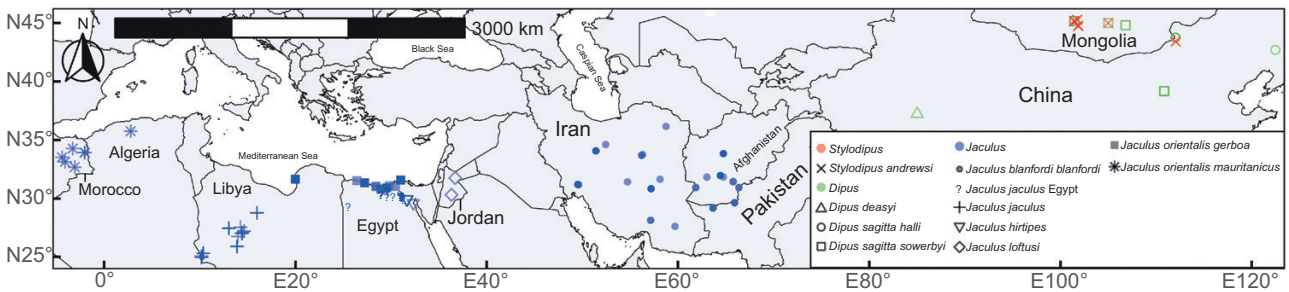

Figure 2. Specimens' localities map. Operational taxonomic units are assigned different symbols/colors (see legend). Geographic WGS84 CRS is used. Locality geographic coordinates appear in Data S1. Map generated using *ggplot* and *rnaturalearth*.

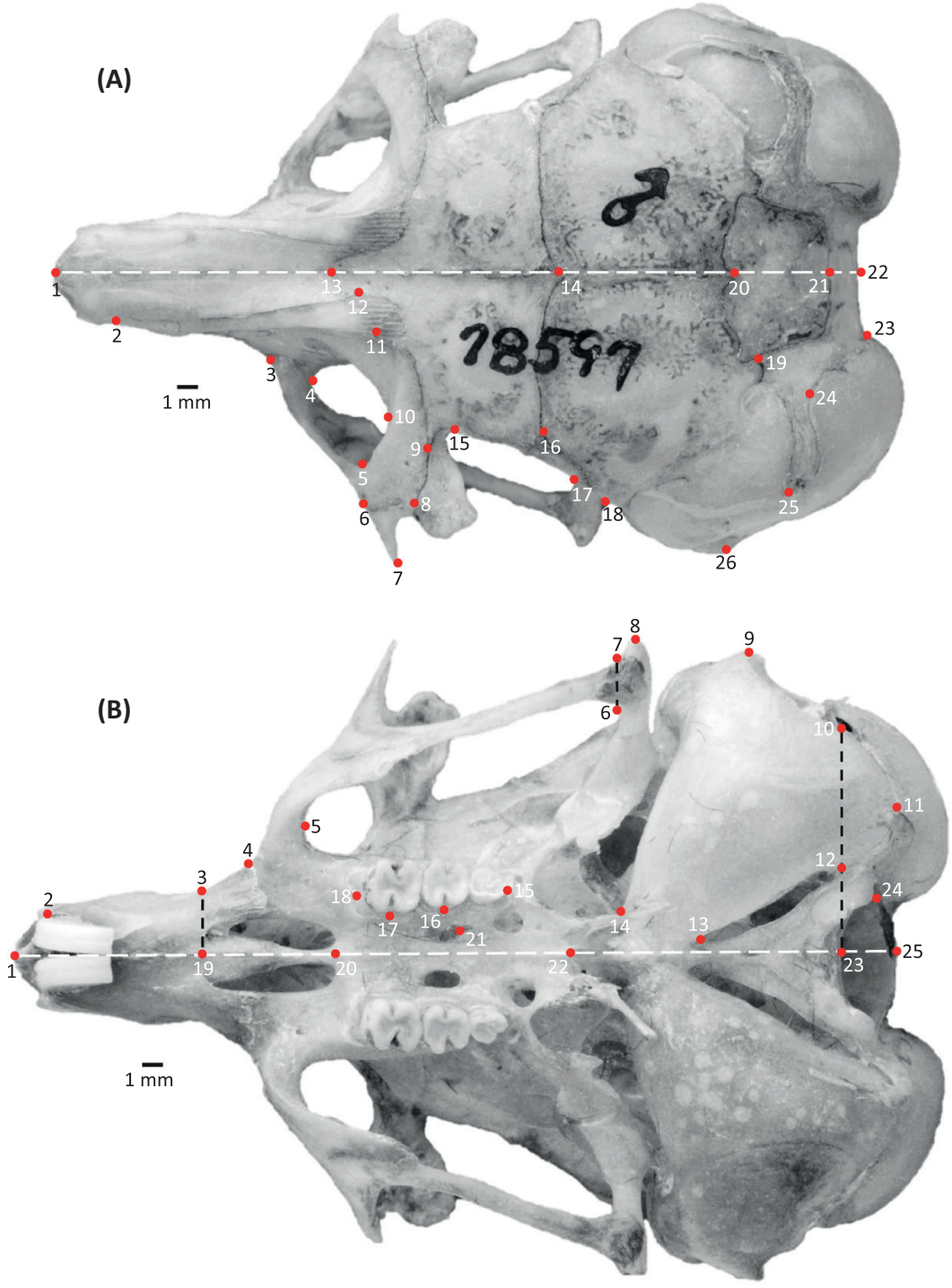

Figure 3. Digitized landmarks on the (A) dorsal and (B) ventral views of the cranium of a lesser Egyptian jerboa (*J. jaculus*; FMNH 78597) from near Siwa Oasis, Egypt. Landmarks are described in Table S1.

mean shape of the sample (for each species separately) and ensuring the absence of outliers.

We calculated measurement error in the digitizing process by digitizing each specimen twice (for each view) and then quantifying the repeatability of both the centroid sizes and the Procrustes shape coordinates. We estimated the repeatability of the centroid sizes by performing an analysis of variance (Anova), a method known as the intraclass correlation coefficient (ICC) in the R package *ICC* (Wolak et al. 2012). We followed the steps in Zelditch et al. (2012) to estimate the repeatability of the Procrustes shape coordinates. This involved calculating the ratio of *among-individual variance* to the sum of *among-individual variance* and *measurement error variance*. We calculated these components based on the mean squares (MS) derived from *geomorph*'s Procrustes Anova (with Procrustes shape coordinates as the response variables and specimen IDs as the predictor variables). As the repeatability of the centroid sizes and the Procrustes coordinates were high (see Results), the averages of these variables across the two trials (of the same specimens) were used in subsequent analyses (see Zelditch et al. 2012).

Statistical analysis

We first assessed sexual size and shape dimorphism by evaluating the influence of OTU identity, sex, and their interaction on centroid sizes and Procrustes shape coordinates via the residual randomization in a permutation procedure (RRPP) in the R library *RRPP*. As we did not detect significant sexual dimorphism (see Results), sex was not considered further.

Next, we constructed RRPP models to assess the effect of (1) OTU identity on cranial size and (2) cranial size, OTU identity, and their interaction on cranial shape—we computed an *F*-distribution Anova table for each model. We then used the *RRPP* library to compare distances between OUT-means based on (1) size, (2) shape, and (3) shape corrected for common allometry (comparisons are between least squares means with logged centroid size as a covariate and no interaction term)—we corrected for common rather than unique allometry as there was evidence of the former, but not the latter in both views (see Results).

We used *ggplot2* to visualize OTU centroid size differences as boxplots and *geomorph* to visualize OTU Procrustes coordinates differences as scatterplots of the first two principal components (PC) of their principal component analysis (PCA). We also generated TPS deformation grids to visualize shapes at PC extremes.

To contrast the cranial shapes of the OTUs more directly, we used *geomorph* to first estimate the mean shape of each OTU and then to perform a GPA on these OTU-mean shapes. This GPA realigns the OTU-mean shapes and computes a Procrustes distance matrix, which we summarized in a UPGMA (unweighted pair group method with arithmetic mean) dendrogram. We visualized differences in OTU-mean shapes as TPS deformations of the mean shape of the OTU-means (i.e. "mean of means") to the mean shape of each OTU—this process gives equal weight to each OTU, regardless of sample size.

According to the RRPP analyses, significant common-OTU allometries were detected in both views (see Results). Hence, we visualized shape-size covariation using a common allometry model in both views by using *geomorph* to plot regression scores (standardized shape scores of the regression of Procrustes shape coordinates on logged centroid sizes) (RegScore; Drake and Klingenberg 2008) against logged centroid sizes. We then generated TPS deformation grids to visualize shapes at RegScore extremes.

Results

The repeatability of the two trials based on the centroid sizes (dorsal ICC = 0.944; ventral ICC = 0.926) was greater than the average repeatability of morphological studies (ICC = 0.65; Wolak et al. 2012). The two trials were also highly repeatable according to the Procrustes coordinates (dorsal score = 0.954; ventral score = 0.961) (scores are explained in the Materials and Methods).

Preliminary models detected no significant sexual size or shape dimorphism in the ventral view—both the main effect (sex) and its interaction with OTU identity was nonsignificant (both $P > 0.05$; Table S2). Similarly, no significant sexual shape dimorphism was found in the dorsal view ($P > 0.05$ for both the main effect and interaction term; Table S2b). For the dorsal size model, the main effect (sex) was nonsignificant ($P > 0.05$; Table S2a) indicating no overall effect of sex on size. A significant dorsal size-sex interaction effect was detected ($P < 0.05$; Table S2a), suggesting a potential "crossover interaction" (i.e. the effect of OTU identity on dorsal size depends on the sex or vice versa). Yet, as the effect size of this model term is much smaller than that of the OTU term ($Z = 2.04$ vs. 9.44; $R^2 = 0.021$ vs. 0.777; Table S2a), a separate analysis for each sex is not warranted (i.e. the effect size disparity is too high for the analysis to be biologically significant).

The 1-factor size models found significant differences among the OTUs in both views (both $P < 0.05$; $Z = 8.48$–9.07; $R^2 = 0.773$–0.799; Table 1A). In both views, most *Jaculus* species were larger in size than *Stylodipus* and *Dipus*, which in turn overlapped (Figure 4). Post hoc pairwise comparisons found significant size differences ($P < 0.05$) among 22 out of the 36 OTU pairs in the dorsal view and 18 out of 36 OTU pairs in the in the ventral view (Table 2A).

The definitive shape models found significant differences among the OTUs in both views (both $P < 0.05$; $Z = 14.55$–15.22; $R^2 = 0.476$–0.523; Table 1B). Cranial shape was also significantly predicted by its size in both views (both $P < 0.05$; $Z = 3.41$–4.43; $R^2 = 0.006$–0.008; Table 1B). Cranial size did not significantly interact with the OTU factor in its effect on cranial shape in both views ($P > 0.05$; Table 1B). This would suggest shape being predicted by common rather than unique OTU allometric patterns. However, the effect sizes of the size factor are orders of magnitude smaller than that of the OTU factor (see Table 1B), and thus unlikely to play a large role in explaining interspecific shape differences.

Post hoc pairwise comparisons found significant shape differences among most OTU pairs (in both views) both without size correction (all $P < 0.05$; Table 2B) and after correcting for common allometry (all $P < 0.05$; Table 2c). The following OTU pairs are exceptions with nonsignificant shape differences ($P > 0.05$) both with and without size correction: (1) *D. s. halli* and *D. s. sowerbyi* (dorsal view), (2) *J. b. blanfordi* and *J. hirtipes* (both views), (3) *J. hirtipes* and *J. jaculus* (dorsal view), (4) *J. hirtipes* and *J. jaculus* Egypt (dorsal view), (5) *J. jaculus* and *J. jaculus* Egypt (both views), and (6) *J. o. gerboa* and *J. o. mauritanicus* (both views) (Table 2B, 2C).

PC1–2 accounted for ~53% of shape variation (in both views) (Figure 5). Although specimens clustered according to their genus (in both views), intergeneric division was greater in the dorsal view (Figure 5A) than the ventral view (Figure 5B). Within genera, OTUs showed marked clustering according to their identity (particularly in *Jaculus*) (Figure 5). In both views, *Dipus* and *Stylodipus* clustered closer to each other in PC1–2 morphospace than either clustered to *Jaculus* (Figure 5). This result is echoed in the OTU-means UPGMA dendrograms, where two main clusters formed in both views, one comprising (all) *Jaculus* and the other contained *Dipus* + *Stylodipus*, which in turn segregated from each other as subclusters (Figure 6).

Dorsal PC1 robustly differentiates *Jaculus* (PC1 max—right quadrants) from *Dipus* + *Stylodipus* (PC1 min—left quadrants)—the latter are in turn discriminated by nonoverlapping scores, with *Dipus* being more negative (Figure 5A). This result is mirrored in the dorsal OTU-means UPGMA dendrogram with *Jaculus* (all OTUs) forming a cluster distinct from *Stylodipus* + *Dipus* (the two *Dipus* OTUs formed their own subcluster) (Figure 6, top). According to the TPS deformations, this division is associated with *Jaculus* having more caudolaterally broadened cranial vaults and enlarged infraorbital foramina when compared to *Dipus* + *Stylodipus* (with converse shape patterns) (Figure 5A; also see Figure 6,

Table 1. Anova tables for the linear model of (a) the effect of OTU identity on logged cranial size and (b) the effect of logged cranial size, OTU identity, and their interaction on cranial shape (Procrustes shape coordinates), for the dorsal and the ventral views.

	df	SS	MS	R^2	*F*	*Z*	*P*
a. Centroid size (log)							
[Dorsal view]							
OTU	9	1.01898	0.11322	0.77317	81.049	8.4898	**0.001**
Residuals	214	0.29895	0.00140	0.22683			
Total	223	1.31793					
[Ventral view]							
OTU	10	1.29693	0.12969	0.79950	85.732	9.0717	**0.001**
Residuals	215	0.32525	0.00151	0.20050			
Total	225	1.62218					
b. Procrustes shape							
[Dorsal view]							
Size	1	0.00617	0.00617	0.00833	4.448	4.4351	**0.001**
OTU	9	0.35277	0.03920	0.47657	28.267	15.2222	**0.001**
Size × OTU	8	0.01212	0.00151	0.01637	1.092	0.7000	0.251
Residuals	205	0.28426	0.00139	0.38402			
Total	223	0.74022					
[Ventral view]							
Size	1	0.00228	0.00228	0.00628	3.221	3.4177	**0.001**
OTU	10	0.18999	0.01900	0.52309	26.821	14.5596	**0.001**
Size × OTU	9	0.00675	0.00075	0.01859	1.059	0.4844	0.299
Residuals	205	0.14522	0.00071	0.39982			
Total	225	0.36321					

Notes: *df* = degrees of freedom; SS = sums of squares: sequential (type-I) for the centroid size models and hierarchical (type-II) for the models of the Procrustes shape; MS = mean squares; R^2= *R*-squared values; *F* = *F*-values; *Z* = effect sizes (standard deviates of *F* sampling distributions); *P* = *P*-values based on 999 permutations. The fit of each linear model was evaluated using RRPP. Model coefficients were estimated using ordinary least squares (OLS). Significant model terms ($P < 0.05$) are indicated in bold. Specimens damaged in either view were excluded ($N = 224$ for dorsal view models; $N = 226$ for the ventral view models).

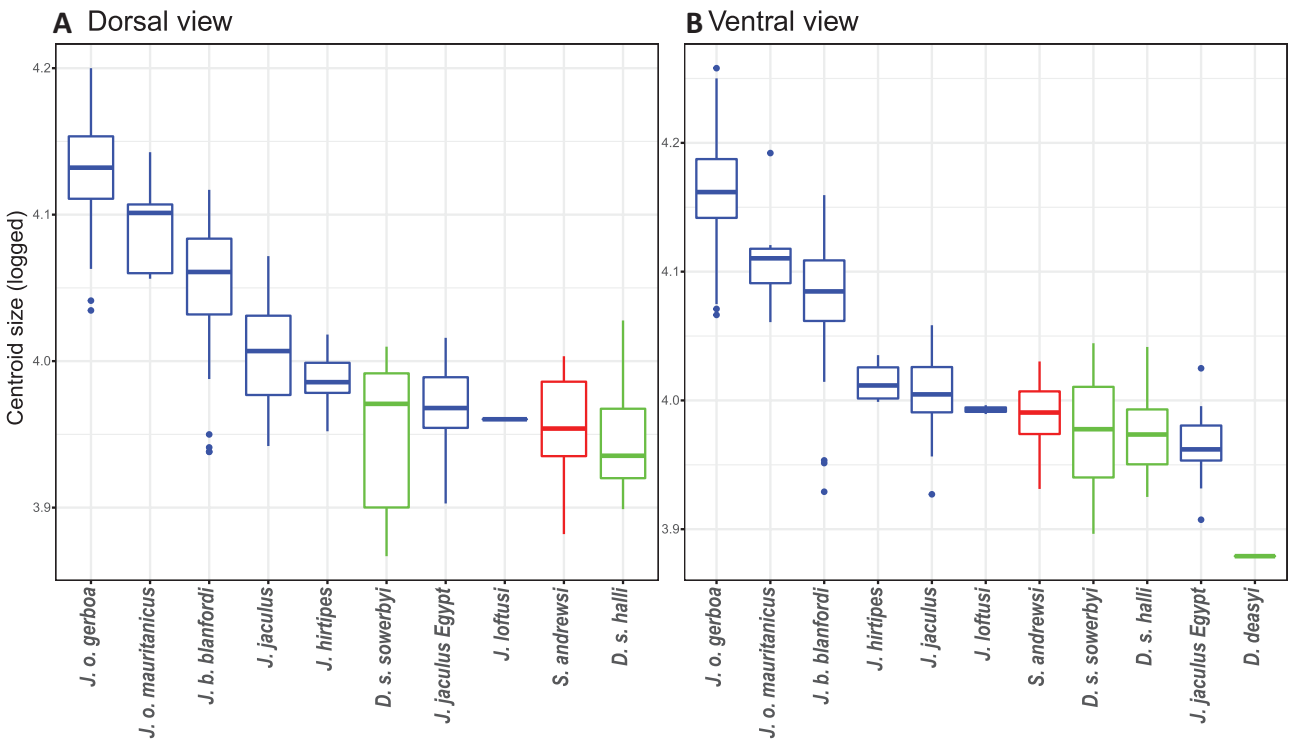

Figure 4. Boxplots of logged cranial centroid sizes of the (A) dorsal and the (B) ventral views of the examined specimens (separated by OTUs). Inner box lines are medians, hinges are first and third quartiles, and whiskers extend to the largest or smallest value (no more than 1.5 times the interquartile range). Individual points past hinges are outliers. Plot generated using *ggplot2*.

Table 2. Pairwise distances between the OUT-means and associated statistics based on (a) logged centroid size, (b) Procrustes shape coordinates, and (c) Procrustes shape coordinates corrected for common allometry.

	(a) Size				(b) Shape (no correction)				(c) Shape (correction)			
	d	UCL	*Z*	*P*	*d*	UCL	*Z*	*P*	*d*	UCL	*Z*	*P*
a. Dorsal view												
D. s. halli — D. s. sowerbyi	0.00	0.06	-1.32	0.971	0.02	0.03	0.35	0.311	0.02	0.03	0.72	0.202
D. s. halli — J. b. blanfordi	0.11	0.04	6.72	**0.001**	0.10	0.02	16.78	**0.001**	0.10	0.03	15.00	**0.001**
D. s. halli — J. hirtipes	0.04	0.07	0.67	0.246	0.10	0.04	10.58	**0.001**	0.10	0.03	11.39	**0.001**
D. s. halli — J. jaculus	0.06	0.04	2.89	**0.014**	0.10	0.02	16.58	**0.001**	0.10	0.02	16.62	**0.001**
D. s. halli — J. jaculus Egypt	0.02	0.05	0.21	0.359	0.10	0.03	14.84	**0.001**	0.10	0.02	16.55	**0.001**
D. s. halli — J. o. gerboa	0.18	0.04	11.91	**0.001**	0.09	0.02	15.91	**0.001**	0.09	0.03	10.26	**0.001**
D. s. halli — J. o. mauritanicus	0.15	0.08	4.87	**0.001**	0.08	0.04	6.19	**0.001**	0.08	0.05	5.44	**0.001**
D. s. halli — S. andrewsi	0.01	0.05	-0.67	0.691	0.07	0.03	9.86	**0.001**	0.07	0.03	10.88	**0.001**
D. s. sowerbyi — J. b. blanfordi	0.10	0.05	5.38	**0.001**	0.10	0.03	15.26	**0.001**	0.10	0.03	13.97	**0.001**
D. s. sowerbyi — J. hirtipes	0.04	0.07	0.47	0.296	0.11	0.04	10.26	**0.001**	0.10	0.04	11.04	**0.001**
D. s. sowerbyi — J. jaculus	0.06	0.05	2.51	**0.023**	0.11	0.03	14.95	**0.001**	0.11	0.03	15.40	**0.001**
D. s. sowerbyi — J. jaculus Egypt	0.02	0.05	-0.06	0.462	0.10	0.03	13.57	**0.001**	0.10	0.03	15.24	**0.001**
D. s. sowerbyi — J. o. gerboa	0.18	0.05	10.38	**0.001**	0.10	0.03	14.92	**0.001**	0.09	0.04	10.18	**0.001**
D. s. sowerbyi — J. o. mauritanicus	0.15	0.08	4.58	**0.001**	0.08	0.04	6.51	**0.001**	0.08	0.05	5.50	**0.002**
D. s. sowerbyi — S. andrewsi	0.01	0.06	-0.83	0.779	0.07	0.03	8.93	**0.001**	0.07	0.03	9.93	**0.001**
J. b. blanfordi — J. hirtipes	0.06	0.06	2.14	**0.028**	0.03	0.03	0.90	0.177	0.03	0.03	1.28	0.115
J. b. blanfordi — J. jaculus	0.05	0.03	3.16	**0.010**	0.04	0.02	6.77	**0.001**	0.04	0.02	7.46	**0.001**
J. b. blanfordi — J. jaculus Egypt	0.08	0.04	5.71	**0.001**	0.03	0.02	5.40	**0.002**	0.04	0.02	4.98	**0.001**
J. b. blanfordi — J. o. gerboa	0.08	0.03	6.95	**0.001**	0.05	0.02	13.17	**0.001**	0.05	0.02	11.24	**0.001**
J. b. blanfordi — J. o. mauritanicus	0.04	0.07	0.52	0.286	0.05	0.04	2.94	**0.019**	0.05	0.04	3.43	**0.005**
J. b. blanfordi — S. andrewsi	0.10	0.04	6.21	**0.001**	0.08	0.02	13.32	**0.001**	0.08	0.03	12.44	**0.001**
J. hirtipes — J. jaculus	0.02	0.06	-0.39	0.570	0.03	0.04	1.42	0.090	0.03	0.03	1.76	0.065
J. hirtipes — J. jaculus Egypt	0.02	0.07	-0.38	0.569	0.03	0.04	1.09	0.147	0.03	0.03	1.45	0.087
J. hirtipes — J. o. gerboa	0.14	0.06	6.29	**0.001**	0.06	0.03	5.56	**0.001**	0.06	0.04	4.57	**0.001**
J. hirtipes — J. o. mauritanicus	0.11	0.09	2.54	**0.023**	0.06	0.05	2.60	**0.026**	0.06	0.05	2.81	**0.017**
J. hirtipes — S. andrewsi	0.03	0.07	0.19	0.348	0.09	0.04	9.28	**0.001**	0.09	0.03	9.87	**0.001**
J. jaculus — J. jaculus Egypt	0.04	0.04	1.65	0.068	0.02	0.02	0.92	0.161	0.02	0.02	0.69	0.207
J. jaculus — J. o. gerboa	0.12	0.03	10.37	**0.001**	0.05	0.02	10.59	**0.001**	0.05	0.02	7.58	**0.001**
J. jaculus — J. o. mauritanicus	0.09	0.07	2.55	**0.019**	0.05	0.04	2.99	**0.013**	0.05	0.04	3.47	**0.005**
J. jaculus — S. andrewsi	0.05	0.04	2.33	**0.027**	0.09	0.02	14.96	**0.001**	0.09	0.02	15.28	**0.001**
J. jaculus Egypt — J. o. gerboa	0.16	0.04	12.32	**0.001**	0.04	0.02	8.17	**0.001**	0.05	0.03	4.59	**0.002**
J. jaculus Egypt — J. o. mauritanicus	0.13	0.08	4.11	**0.003**	0.04	0.04	2.14	**0.033**	0.04	0.04	2.23	**0.038**
J. jaculus Egypt — S. andrewsi	0.01	0.05	-0.41	0.577	0.09	0.03	13.26	**0.001**	0.08	0.02	14.99	**0.001**

Table 2. Continued

	(a) Size				(b) Shape (no correction)				(c) Shape (correction)			
	d	UCL	*Z*	*P*	*d*	UCL	*Z*	*P*	*d*	UCL	*Z*	*P*
J. o. gerboa — J. o. mauritanicus	0.04	0.07	0.27	0.341	0.03	0.04	-0.09	0.469	0.03	0.04	0.01	0.429
J. o. gerboa — S. andrewsi	0.17	0.04	11.42	**0.001**	0.09	0.02	15.18	**0.001**	0.08	0.03	9.86	**0.001**
J. o. mauritanicus — S. andrewsi	0.14	0.08	4.43	**0.002**	0.07	0.04	5.59	**0.001**	0.07	0.04	4.84	**0.002**
b. Ventral view												
D. s. halli — D. s. sowerbyi	0.00	0.06	-1.19	0.910	0.02	0.02	2.19	**0.032**	0.02	0.02	2.35	**0.035**
D. s. halli — J. b. blanfordi	0.10	0.05	5.78	**0.002**	0.07	0.02	16.29	**0.001**	0.07	0.02	13.07	**0.001**
D. s. halli — J. hirtipes	0.04	0.08	0.21	0.350	0.07	0.03	9.90	**0.001**	0.07	0.03	9.12	**0.001**
D. s. halli — J. jaculus	0.03	0.05	0.56	0.237	0.07	0.02	16.43	**0.001**	0.07	0.02	16.21	**0.001**
D. s. halli — J. jaculus Egypt	0.01	0.05	-0.52	0.623	0.07	0.02	14.85	**0.001**	0.07	0.02	14.81	**0.001**
D. s. halli — J. o. gerboa	0.19	0.05	10.94	**0.001**	0.05	0.02	13.06	**0.001**	0.05	0.03	7.33	**0.001**
D. s. halli — J. o. mauritanicus	0.14	0.07	4.65	**0.001**	0.04	0.03	5.84	**0.001**	0.04	0.03	4.14	**0.002**
D. s. halli — S. andrewsi	0.01	0.05	-0.74	0.735	0.05	0.02	9.72	**0.001**	0.05	0.02	9.74	**0.001**
D. s. sowerbyi — J. b. blanfordi	0.10	0.05	5.73	**0.001**	0.06	0.02	13.56	**0.001**	0.06	0.02	11.62	**0.001**
D. s. sowerbyi — J. hirtipes	0.04	0.08	0.36	0.317	0.06	0.03	8.16	**0.001**	0.06	0.03	8.24	**0.001**
D. s. sowerbyi — J. jaculus	0.03	0.05	0.68	0.236	0.07	0.02	14.85	**0.001**	0.07	0.02	14.98	**0.001**
D. s. sowerbyi — J. jaculus Egypt	0.01	0.05	-0.81	0.766	0.07	0.02	13.32	**0.001**	0.07	0.02	13.72	**0.001**
D. s. sowerbyi — J. o. gerboa	0.19	0.05	10.81	**0.001**	0.05	0.02	12.02	**0.001**	0.05	0.03	6.97	**0.001**
D. s. sowerbyi — J. o. mauritanicus	0.14	0.07	4.66	**0.001**	0.05	0.03	5.54	**0.001**	0.04	0.03	3.90	**0.005**
D. s. sowerbyi — S. andrewsi	0.01	0.06	-0.60	0.681	0.04	0.02	6.79	**0.002**	0.04	0.02	6.87	**0.001**
J. b. blanfordi — J. hirtipes	0.06	0.07	1.50	0.089	0.02	0.02	0.10	0.402	0.02	0.03	0.25	0.330
J. b. blanfordi — J. jaculus	0.07	0.04	4.73	**0.002**	0.03	0.01	7.02	**0.001**	0.03	0.01	5.94	**0.002**
J. b. blanfordi — J. jaculus Egypt	0.11	0.04	7.47	**0.001**	0.02	0.01	5.45	**0.001**	0.03	0.02	3.82	**0.003**
J. b. blanfordi — J. o. gerboa	0.08	0.03	7.09	**0.001**	0.03	0.01	10.77	**0.001**	0.03	0.01	7.42	**0.001**
J. b. blanfordi — J. o. mauritanicus	0.03	0.07	0.33	0.331	0.04	0.02	5.59	**0.001**	0.04	0.02	5.05	**0.001**
J. b. blanfordi — S. andrewsi	0.09	0.05	5.02	**0.001**	0.06	0.02	14.05	**0.001**	0.06	0.02	12.73	**0.001**
J. hirtipes — J. jaculus	0.01	0.07	-0.92	0.803	0.03	0.03	2.70	**0.021**	0.03	0.03	2.63	**0.024**
J. hirtipes — J. jaculus Egypt	0.05	0.07	0.83	0.190	0.03	0.03	2.50	**0.024**	0.03	0.03	2.27	**0.030**
J. hirtipes — J. o. gerboa	0.15	0.07	5.25	**0.001**	0.03	0.03	3.81	**0.003**	0.03	0.03	2.37	**0.032**
J. hirtipes — J. o. mauritanicus	0.10	0.09	1.97	**0.045**	0.04	0.03	3.30	**0.005**	0.04	0.04	2.61	**0.025**
J. hirtipes — S. andrewsi	0.03	0.08	-0.18	0.488	0.06	0.03	7.66	**0.001**	0.06	0.03	7.30	**0.001**
J. jaculus — J. jaculus Egypt	0.04	0.04	1.72	0.069	0.01	0.02	1.07	0.133	0.01	0.02	1.14	0.139
J. jaculus — J. o. gerboa	0.16	0.04	11.57	**0.001**	0.04	0.01	11.54	**0.001**	0.04	0.02	6.15	**0.001**
J. jaculus — J. o. mauritanicus	0.11	0.07	3.77	**0.002**	0.05	0.02	7.04	**0.001**	0.05	0.03	5.45	**0.001**
J. jaculus — S. andrewsi	0.02	0.05	-0.10	0.446	0.08	0.02	16.43	**0.001**	0.08	0.02	16.75	**0.001**
J. jaculus Egypt — J. o. gerboa	0.20	0.04	13.47	**0.001**	0.03	0.01	7.92	**0.001**	0.03	0.03	3.10	**0.013**
J. jaculus Egypt — J. o. mauritanicus	0.15	0.07	5.40	**0.001**	0.04	0.03	5.56	**0.001**	0.04	0.03	3.79	**0.004**

Table 2. Continued

	(a) Size				(b) Shape (no correction)				(c) Shape (correction)			
	d	UCL	*Z*	*P*	*d*	UCL	*Z*	*P*	*d*	UCL	*Z*	*P*
J. jaculus Egypt — S. andrewsi	0.02	0.05	0.13	0.369	0.07	0.02	15.28	**0.001**	0.07	0.02	14.68	**0.001**
J. o. gerboa — J. o. mauritanicus	0.05	0.06	1.16	0.133	0.02	0.02	0.85	0.180	0.02	0.02	1.06	0.131
J. o. gerboa — S. andrewsi	0.18	0.04	10.84	**0.001**	0.05	0.02	13.65	**0.001**	0.06	0.02	8.73	**0.001**
J. o. mauritanicus — S. andrewsi	0.13	0.07	4.20	**0.001**	0.05	0.03	6.31	**0.001**	0.05	0.03	5.23	**0.002**

Notes: *d* = distances between (least squares) means; UCL = 95% upper confidence limit for *d* (one-tailed); *Z* = effect sizes; *P* = *P*-values based on 999 permutations. Significantly different pairs ($P < 0.05$) are in bold. Specimens damaged in either view were excluded from the particular view. OTUs represented by $N < 5$ specimens were not included in pairwise comparisons. Procrustes shape coordinates corrected for common allometry (correction) indicate that comparisons are between least squares means with logged centroid size as a covariate and no interaction term.

top). Dorsal PC2 differentiates *J. orientalis* (2 OTUs) (PC2 min—lower quadrants) from other *Jaculus* (PC2 max—upper quadrants) (Figure 5A). This result is mirrored to some extent in the dorsal OTU-means UPGMA dendrogram, with *Jaculus* OTUs subclustering into (1) *J. loftusi*, (2) *J. orientalis* (2 OTUs), (3) *J. jaculus* (2 OTUs), and (4) *J. blanfordi* + *J. hirtipes* (Figure 6, top). The TPS deformations indicate that when compared to other *Jaculus*, *J. orientalis* have broadened faces (particularly rostra and infraorbital foramina) at the expense of caudal cranial vault ends (Figure 5A; also see Figure 6, top).

Ventral PC1 also differentiates *Jaculus* (closer to PC1 min) from *Stylodipus* + *Dipus* (closer to PC1 max)—the former is in turn partly subdivided, with *J. orientalis* (2 OTUs) having more intermediate scores than other *Jaculus* (with more negative scores) (Figure 5B). This result is also observed in the ventral OTU-means UPGMA dendrogram with *Jaculus* (all OTUs) forming a cluster (with the 2 *J. orientalis* OTUs forming a subcluster, and all other *Jaculus* forming another subcluster) distinct from *Stylodipus* + *Dipus* (the 3 *Dipus* OTUs formed their own subcluster) (Figure 6, bottom). Based on the TPS deformations, this separation is associated with *Jaculus* having more caudolaterally expanded cranial bases (tympanic bullae project beyond foramina magna) along with reduced molar rows and rostra when compared to *Stylodipus* + *Dipus* (with converse shape patterns) (Figure 5B; also see Figure 6, bottom). Ventral PC2 showed ambiguous differentiation with minor clustering among OTUs (e.g. higher scores in *Stylodipus* + *J. blanford* when compared to the other taxa); however, TPS deformations show no clear differences along the axis extremes, except perhaps somewhat larger bullae and smaller orbits toward PC2 max (Figure 5B).

According to the RegScore plot, relative to small crania (RegScore min), the main distinguishing features of large crania (RegScore max) are more rostromedially compressed cranial vaults (Figure 7A) and perhaps slightly larger orbits and smaller molar rows (Figure 7B).

Discussion

Our cranial dataset clearly discerns most OTU pairs, many of which show pronounced size and/or shape differences, particularly at higher taxonomic levels. *Jaculus* is the largest of the sampled genera; *Stylodipus* and *Dipus* largely overlapped in size. This result, along with the observed intrageneric differences, is as expected given previously reported dipodine body size differences, that is, *J. orientalis* is the largest of the genus, followed by *J. blanfordi*, and then *J. jaculus* (see Nowak and Paradiso 1983). While the cranial sizes of the 2 *J. orientalis* subspecies were largely nonoverlapping (*J. o. gerboa* being the larger of the two—see Figure 4), this difference was not statistically significant. This was not the case for the other subspecies (which overlapped in size), suggesting that this trait is not taxonomically informative. This further discourages the use of traditional distance-based cranial morphometrics in dipodine taxonomy, as it tends to be highly driven by size. Nonetheless, these linear cranial measurements (including those related to the size and shape of the overall skull, along with particular substructures, e.g. auditory bulla, zygomata, braincase, infraorbital foramina, rostrum including nasals, molars) forms the basis of much of the traditional taxonomy of this group, reaching as narrow as the

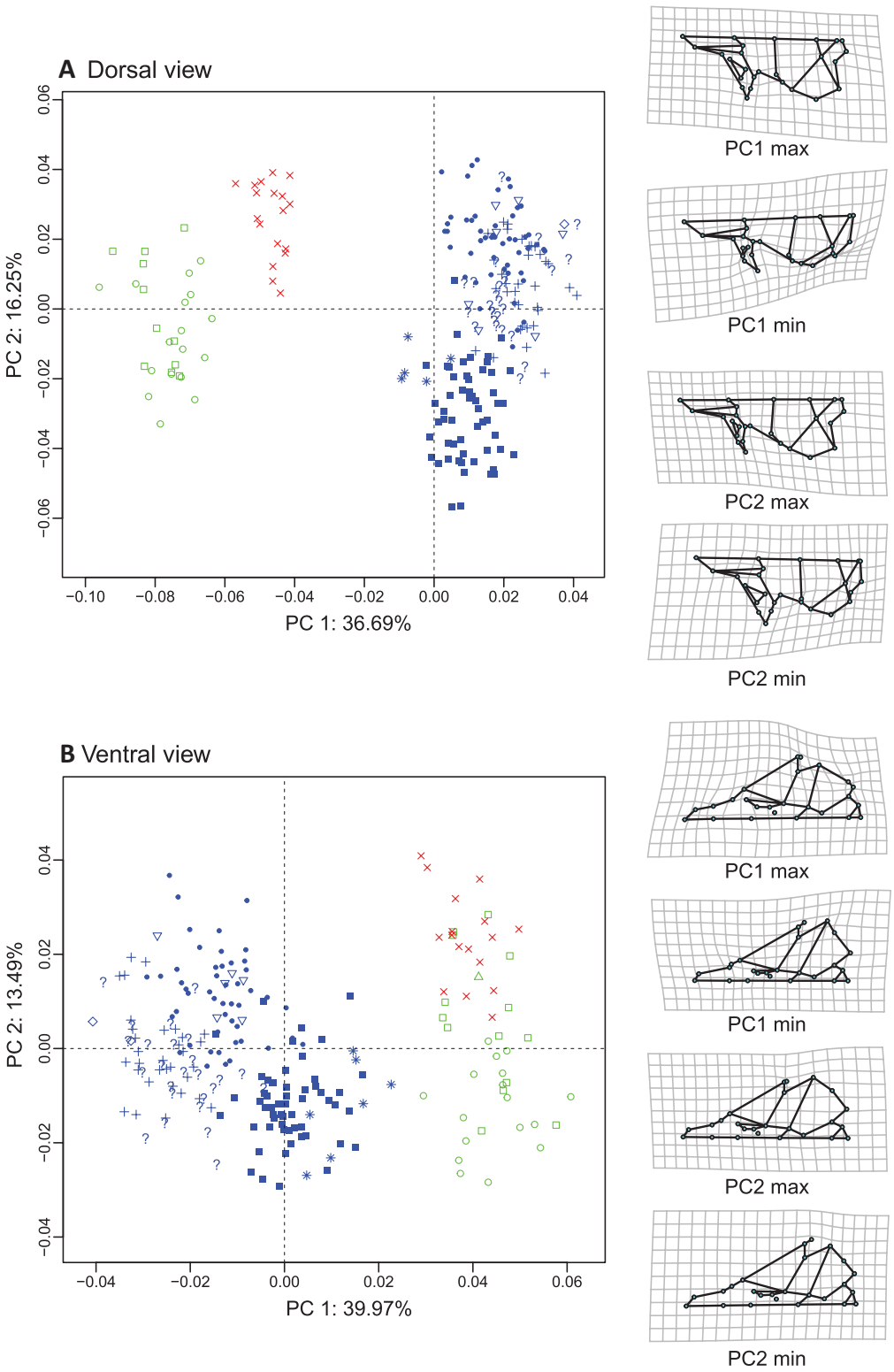

Figure 5. Principal component analysis scatterplots based on the cranial Procrustes shape coordinates of the (A) dorsal and the (B) ventral views of the examined specimens (separated by OTUs). The percent of total variation explained by the principal components (PC1-2) are shown. Genera are designated by different colors, and OTUs by different symbols (following the legend in Figure 2). Principal component origins are indicated with dotted lines. Thin-plate spline deformation grids show shapes at axis extremes, all of which (in both views) are magnified 1.5× fold to better elucidate the differences Landmarks are linked to aid visualization. Plot generated using *geomorph*.

subspecific level, especially in *Jaculus* (Setzer 1956; Happold 1967; Ranck 1968). Interspecific size variation does not conform to Bergmann's (1847) rule, which predicts larger sizes in higher latitudes (with colder climates), and is perhaps driven by resource availability, which is shown to be applicable to certain rodent taxa (see Alhajeri et al. 2020b). For example, within *Jaculus*, the largest species *J. orientalis* occurs in more productive regions along the south Mediterranean coast than

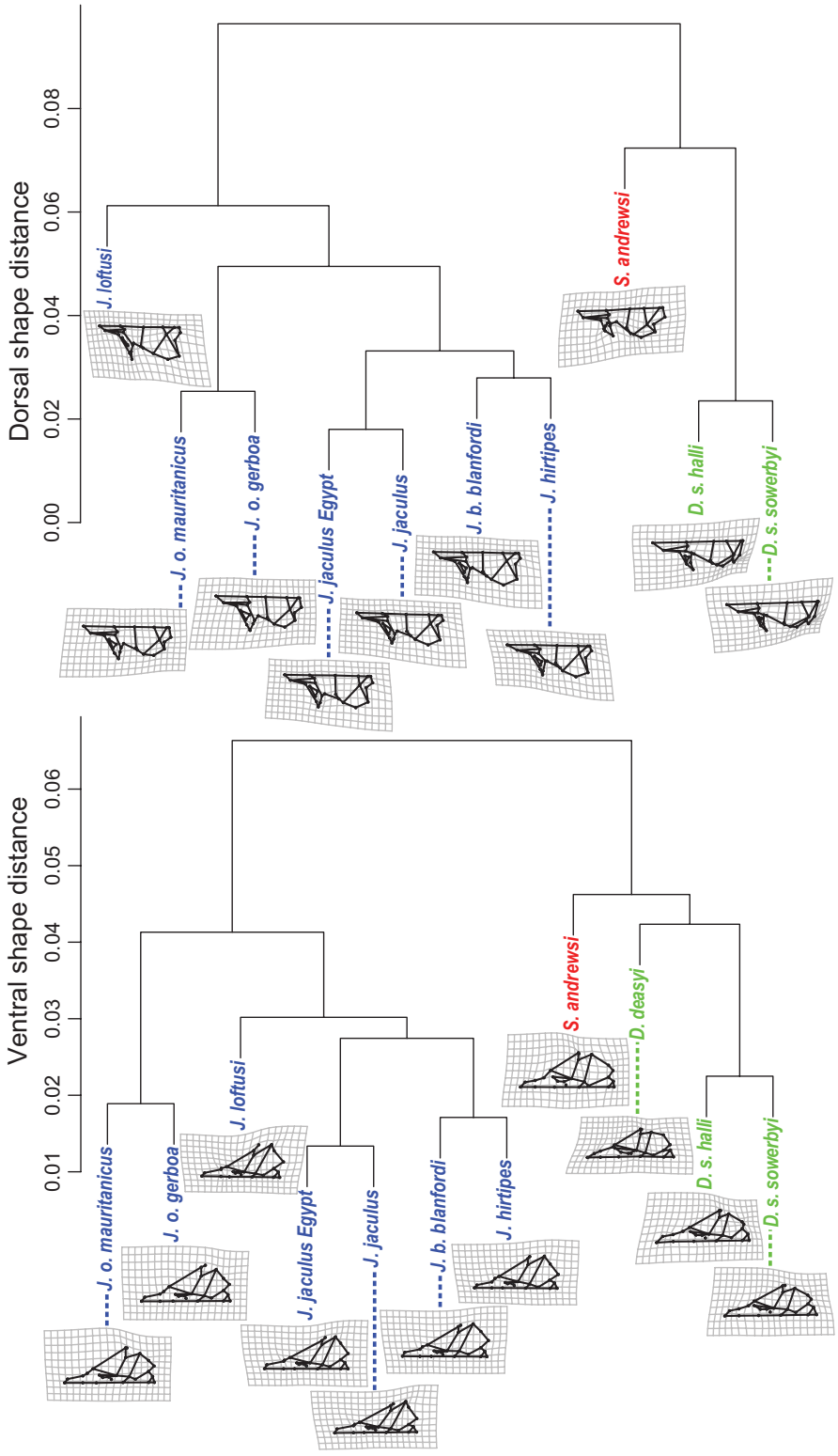

Figure 6. UPGMA dendrograms based on the cranial Procrustes shape coordinates of the (top) dorsal and the (bottom) ventral views of the examined specimens (separated by OTUs). The dendrograms show similarities in OTU-mean shapes along with associated TPS deformation grids for each OTU (compared to the average of the OTU-mean shapes). To aid visualization, landmarks are linked, and deformations are magnified 2-fold (in both views). The shape distance for both views is also indicated. Figure generated using base R functions and *geomorph*.

the smallest species *J. jaculus* which occurs in the interior of the Saharan desert (*J. blanfordi* occurs in the Irano-Turanian region) (Shenbrot et al. 2008).

Some of the identified shape differences among the OTUs were driven by allometry. The patterns that we detected, particularly in the dorsal view, were consistent with the rule of craniofacial evolutionary allometry (CREA; Cardini and Polly 2013), which predicts relatively longer faces and smaller braincases in larger mammalian species (driven by constraints on skull structure) (also see Cardini et al. 2015; Cardini

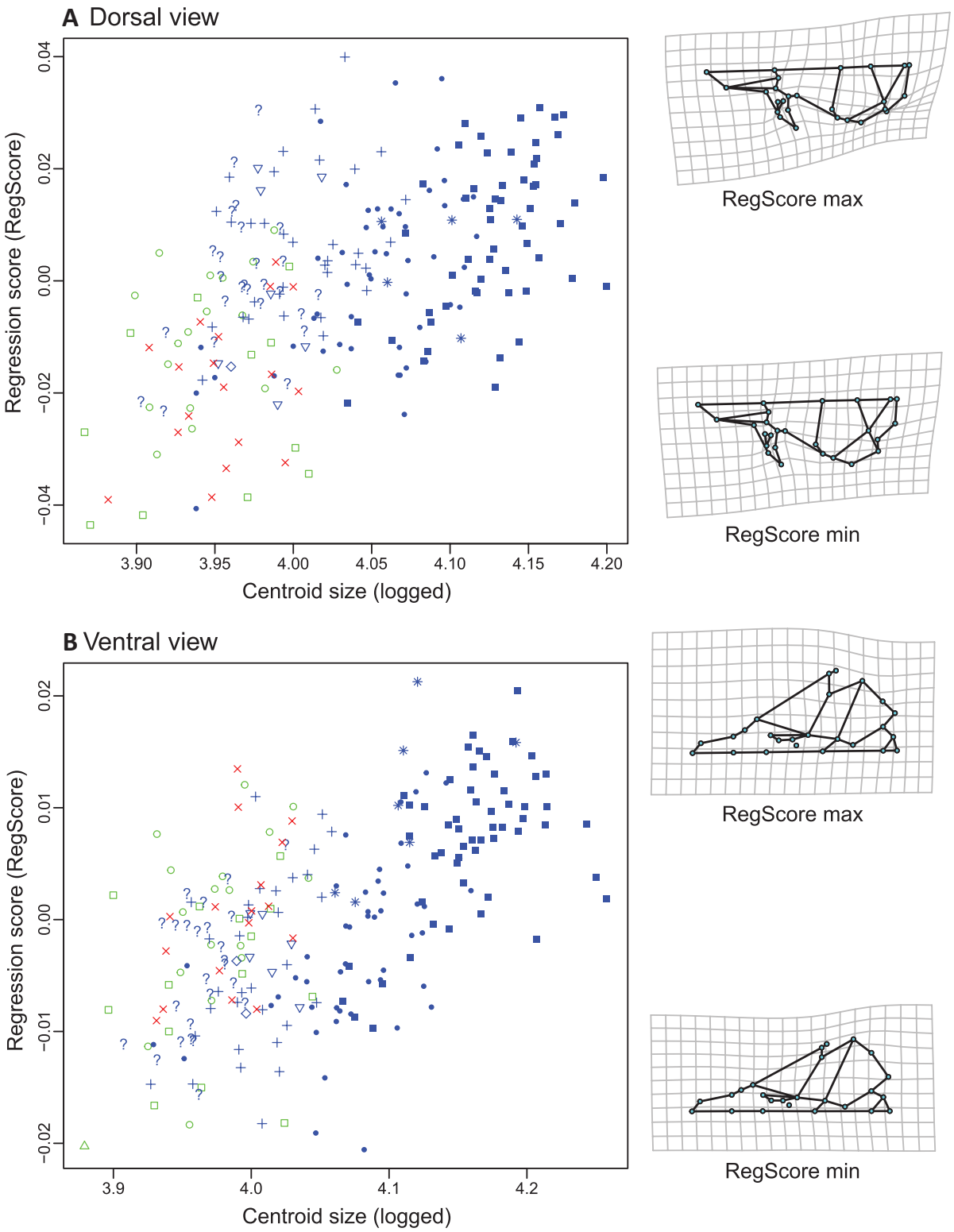

Figure 7. Shape-size covariation scatterplots based on the cranial Procrustes shape coordinates of the (A) dorsal and the (B) ventral views of the examined specimens (separated by OTUs). The axes show the standardized shape scores from the regression of shape (Procrustes shape coordinates) on size (logged centroid sizes) (RegScore; Drake and Klingenberg 2008) plotted vs. logged centroid sizes. Genera are designated with different colors, and OTUs are with different symbols (following the legend in Figure 2). TPS deformation grids show shapes at axis extremes. To aid visualization, landmarks are linked, and deformations are magnified 2-fold (in both views). The common allometry shape-size covariation model (shape ~ size + OTU) was used for both views as it was the best fit allometry model—see Table 1 and the Materials and Methods for more information. Plot generated using *geomorph*.

2019). We previously found similar results in other desert rodents (Alhajeri 2021c, 2022b) supporting the robustness of this allometric pattern. Despite cranial shape being predicted by its size, clearly it is not the main determining factor, that is, the "OTU" factor explains more variation (see Table 1 and the 'Results' section).

The species-level cranial shapes detected in this study (Figures 5 and 6) are consistent with those previously reported in the literature. For example, distinguishing features of dipodid crania described by Kingdon et al. (2013) include hypertrophied auditory bullae, compressed nasals, well-developed jugal plates, and expanded masseters (passing through large infraorbital foramen)—these can be clearly observed in Figure 6. Within dipodines, Michaux and Shenbrot (2017) described the auditory bullae as being relatively reduced and simpler (1-chambered) in the "primitive" *Dipus* and *Stylodipus* when compared to the "advanced" *Jaculus*, where it is more inflated and multichambered. We find similar patterns; *Jaculus* clustered in PC1 max in the dorsal view and PC1 min in the ventral view, which according to the TPS deformations (of both views) is associated with laterocaudally enlarged auditory bullae, which extend beyond the foramen magnum in the ventral view, and beyond the jugal plate in the dorsal view (Figure 5). *Dipus* and *Stylodipus* clustered in PC1 min in the dorsal view and PC1 max in the ventral view, which is associated with more modest bullae and cranial vaults. The especially inflated auditory bullae of *Jaculus* are perhaps a consequence of the concurrent hypertrophy of both the tympanic and the mastoid portions (the latter is the largest of the 2), when compared with the expansion of just the tympanic in *Dipus* and *Stylodipus* (Shenbrot et al. 2008). Bulla size is often associated with hearing ability in mammals (e.g. Taylor et al. 2021; Scarpitti and Calede 2022), and its hypertrophy is a common adaptation in desert rodents aiding in sound detection (and thus escaping predators) in open habitats (Lay 1972; Webster and Webster 1975). The GMM analyses allowed us to notice additional perhaps more subtle differences between these 2 major groups (only evident after scaling), with *Jaculus* also differing from the other 2 genera by its wider, but shorter skull, slenderer rostrum, larger infraorbital foramen (when viewed dorsally), more laterally projecting maxilla and jugal, wider, but shorter frontal and parietal, narrower interparietal, smaller occipital, smaller molars, and wider, but shorter tympanic bullae (Figure 5). Overall, this indicates that GMM facilitates the detection of more minute patterns, which seems to also be useful at narrower taxonomic scales (see below).

The resemblance of *Dipus* and *Stylodipus* crania is evident in their relative proximity in PC1–2 morphospace, and their clustering together in the UPGMA dendrograms. This similarity was first mentioned in the original description of the species (Allen 1925), with the author mostly distinguishing *Stylodipus* from *Dipus* cranially by its larger auditory bulla, particularly in its dorsal and posterior portion, which consequently compresses nearby bones, such as the occipital. The relatively larger bulla size of *Stylodipus* can be clearly observed when comparing the species means (Figure 6), where some rostrocaudal compression can also be seen anterior to the bulla, and also in the dorsal PCA plot, where it takes an intermediate position along PC1, between *Dipus* and *Jaculus* (Figure 5A). Convergent adaptations are very common in desert rodents (Mares 1976, 1980; Berman 1985), and overlap among genera in the PCA plots could reflect such convergence to similar habitat substrate. For example, *Dipus* and *Stylodipus* (and *J. jaculus*) are habitat generalists (i.e. can use sand, gravel, and clay substrates), while *J. blanfordi* and *J. orientalis* are hard substrate (i.e. clay) specialists (Michaux and Shenbrot 2017). This could partly explain their overlap in PCA morphospace, partly explained by smaller rostra and incisors, when compared to *Jaculus* which has larger more robust rostra and incisors (see tip of rostrum which has the roots of the incisors) which apparently facilitates burrowing through harder substrate (see below). Convergent skull adaptations to hard soils have been observed in other rodent taxa, including pocket gophers (see Marcy et al. 2016). Fossoriality exerts a selective pressure not only on the skull, but also on other parts of the body, including the appendicular skeleton, particularly in desert rodents (Tavares et al. 2020).

In addition to these previously reported patterns, this study highlights potentially newly noticed cranial differences, such as the *Stylodipus* skull (when compared to *Dipus*) having a somewhat slenderer rostrum, narrower, less laterally projecting maxilla and jugal, narrower frontal, wider cranial vault (including the parietal), smaller foramen magnum, and larger molars (Figure 6). These apparently newly observed set of cranial differences increase confidence in the phylogenetic perspectives based on DNA sequences and karyotypes (see Lebedev et al. 2013) along with the male genitalia (see Shenbrot et al. 2008), which find *Stylodipus* to be more closely related to *Jaculus* than either is to *Dipus* (Figure 1). This may indicate that their superficial resemblance could be a result of convergence. Indeed, according to Shenbrot et al. (2008), *Stylodipus* and *Dipus* have the least specialized locomotion among dipodines, while *Jaculus* is the most specialized. These authors also consider *Stylodipus* and *Dipus* as having the least developed teeth, skull, bullae, and genitalia, while *Jaculus* has among the most developed. Dental variation, however, does not seem to be associated with diet, as molar height (not measured in this study) tends to be low-crowned in *Dipus*, whose diet tends to be generalized herbivory, while it is medium crowned in *Stylodipus* and *Jaculus*, whose diet includes mostly seeds and green plant parts (Shenbrot et al. 2008). Alternatively, their cranial convergence could be related shared climate, as their ranges appear to overlap in northern China and Mongolia (see Michaux and Shenbrot 2017), and rodents' morphology seems to be highly responsive to climate (Alhajeri et al. 2020a; Kang et al. 2020; Nokelainen et al. 2020; Prado et al. 2022).

Operational taxonomic units largely clustered according to their genus, particularly at the dorsal view (the ventral view, being comprised of such structures as the teeth and bullae, is likely more impacted by environmental adaptations—see below). One of the main divisions at the intrageneric level is *J. orientalis* being differentiated from its congeners by its overall wider skull, including broader rostrum, wider and more laterally projecting maxilla and jugal, enlarged infraorbital foreman, wider frontals and parietals, along with relatively smaller tympanic bulla, and larger orbits (Figures 5 and 6). *Jaculus orientalis* is traditionally differentiated from its congeners by its overall greater size and thus greater external and cranial measurements, but also in fur color, and other unique cranial features, such as those related to the mastoid and the nasals (Osborn and Helmy 1980). The difference between *J. orientalis* and congeners is not unexpected given its phylogenetic placement at the base of the genus, being sister to all its congeners (Figure 1). However, *J. orientalis* is often grouped with *J. blanfordi* in subgenus *Haltomys* Brandt, 1844 (while the remaining congeners *J. hirtipes* + *J. loftusi* + *J. jaculus* are placed in the subgenus *Jaculus*) (Michaux and Shenbrot 2017). We do not find support for this taxonomic arrangement, as the cranial morphology of *J. blanfordi* (after accounting for scale) resembles species in the subgenus *Jaculus* (*J. hirtipes* in particular) more than *J. orientalis* as evidenced by both their position in PC morphospace and the species means dendrograms (Figures 5 and 6). This is somewhat consistent

with Ranck's (1968) prior observation that *J. blanfordi* can be recognized by its less inflated bulla, although the author also noted other skull differences not examined in this study, such as skull flatness, zygomata fragility, and the oval foramina. Thus, the superficial resemblance of the 2 *Haltomys* species is perhaps due to their being both larger than the other *Jaculus*, and thus partly explained by shared allometric patterns. However, the 2 *Haltomys* do share other noncranial characters, such as those of the upper molars and male genitalia (Shenbrot et al. 2008). Alternatively, their resemblance could be partly explained by their ecological specializations. Within genus *Jaculus*, *J. blanfordi* is most specialized compact soil, followed by *J. orientalis*, and lastly by *J. jaculus*—specialization is often accompanied by increasingly large rostra (and larger incisors) to aid in digging harder ground (Shenbrot et al. 2008). Moreover, the habitat of *J. orientalis* differs from that of *J. jaculus* in being less arid and with more plant cover, often close to the Mediterranean coast (Kingdon et al. 2013). *Jaculus orientalis gerboa* and *J. o. mauritanicus* showed no significant differences in cranial shape, despite previous reports that these subspecies correspond with allopatric genetic clades (see Ben Faleh et al. 2016; Michaux and Shenbrot 2017).

Among the sampled OTUs in the subgenus *Jaculus*, *J. jaculus* did not significantly differ from *J. jaculus* Egypt in both views, suggesting that the latter does not consist of many (if any) *J. hirtipes* specimens (see the "Materials and Methods"). Both *J. jaculus* OTUs also did not significantly differ from *J. hirtipes* in the dorsal view (the latter did not significantly differ from *J. b. blanfordi* in both views). However, *J. loftusi* was clearly distinct from all congeners, being characterized by a shorter rostrum, smaller infraorbital foramen, a more caudolaterally expanded tympanic bulla, and a somewhat more laterally projecting zygomatic process (Figure 6). This result does not recapitulate phylogenetic proximity, as *J. loftusi* is phylogenetically more closely related to *J. hirtipes* than it is to *J. jaculus* (see Michaux and Shenbrot 2017).

The three sampled *Dipus* OTUs overlapped in PC morphospace (Figure 5), with *D. s. halli* not significantly differing from *D. s. sowerbyi* in the dorsal view. The mean shapes of these 2 subspecies are also almost indistinguishable from each other in both views (Figure 6). In the original description of *D. halli*, it was mainly differentiated from *D. sowerbyi* by its larger size (Sowerby 1920). Not only was this difference in size not detected (Figure 4), after accounting for scale, cranial shapes were found not to differ in a meaningful manner either (Figure 6). Interestingly, and notwithstanding the inclusion of a single specimen, the ventral shape of *D. deasyi* (dorsal view broken) differed from the mean shape of the other sampled *Dipus*, including the former having an overall larger molar row, a somewhat more inflated tympanic bulla, and a relatively shorter, slenderer rostrum (Figure 6). This is in accordance with newer phylogenetic findings that increasingly support the idea of considering *D. deasyi* to be a full species, as it is genetically divergent from all other *Dipus* subspecies (Cheng et al. 2018; Lebedev et al. 2018). According to Lebedev et al. (2018), the original description of *D. deasyi* mentions the large molars that we detected in this study, while according to Sowerby (1920), the "muzzle" of *D. deasyi* is narrower than that of *D. sowerbyi*, both of which are in agreement with the patterns detected in the present study. However, the larger tympanic bulla that we detected is in disagreement with Thomas (1908), who described the bullae of *D. sowerbyi* as being larger than those of *D. deasyi*. This could either be a consequence of the differences in the measurements of this structure (i.e. whether or not to include the mastoid part of the bulla in measuring the auditory bulla) or whether or not to account for scale (i.e. not done in traditional measurements). The larger molars of *D. deasyi* could potentially be driven by dietary differences, for example., in other rodents, increasing molar size, particularly M3, is associated with increased herbivory (Ronez et al. 2020). Variation in the bulla and the rostrum in rodents are commonly associated with climate and substrate, respectively, as previously discussed.

In conclusion, we found significant size and shape differences among most dipodine OTU pairs. Crania were not sexually dimorphic. Common allometry explained a significant, yet small, amount of shape variation. Specimens clustered according to their OTU identity, with *Dipus* and *Stylodipus* showing more resemblance to each other than either is to *Jaculus*. *J. orientalis* greatly differed from other *Jaculus*. *Jaculus blanfordi*, a member of the subgenus *Haltomys*, resembles members of the subgenus *Jaculus* more than its consubgeneric *J. orientalis*. The cranial shape of *J. loftusi* was clearly distinct from its congeners. Cranial shapes of *D. s. halli* and *D. s. sowerbyi* were indistinguishable, but they clearly differed from that of *D. deasyi*. Some of the shape variation was accounted for by phylogeny, but ecological convergence (particularly to habitat substrate), also played a role.

Acknowledgments

The authors are indebted to the following museum curators, collection managers, and staff for permitting access to their collections and general assistance: AMNH (Ms. Marisa Surovy, Ms. Eleanor Hoeger, and Ms. Eileen Westwig), FMNH (Dr. Bruce Patterson, Dr. Lawrence Heaney, Dr. Adam Ferguson, Mr. John Phelps, Mr. William Stanley, and Ms. Lauren Smith), MVZ (Dr. Christopher Conroy, Dr. James Patton, and Dr. Eileen Lacey), and USNM (Mr. Darrin Lunde and Dr. Michael Carleton). We thank the three anonymous referees for their helpful comments. A small portion of the travel expenses to BHA was covered by Kuwait University as part of a scientific leave that took place in 2019–2020.

Funding

No grant funding was received for this project.

Conflict of Interest

The authors declare no conflict of interest.

Author Contributions

BHA conceived and designed the study, photographed the specimens, ran the analyses, and wrote the manuscript. ZH collected the morphometric data. BHA, ZH, and HA revised the manuscript. All authors read and approved the final version of the manuscript.

Data Availability

All data generated in this study are deposited in the supporting information (Data S1).

Supplementary Material

Supplementary material can be found at https://academic.oup.com/cz.

Appendix A

The specimens examined in this study (N = 235). See the Materials and methods for museum abbreviations.

Dipus deasyi (N = 1)

USNM 573127.

Dipus sagitta halli (N = 18)

AMNH 58556, 58557, 58558, 58562, 58563, 58574, 58576, 58577, 58578, 58579, 58585, 58587, 58588, 58589, 58590; FMNH 30323, 30325; USNM 544449.

Dipus sagitta sowerbyi (N = 14)

AMNH 58608, 58614, 58623, 84121, 84135; FMNH 30319, 30320, 30334, 30335; USNM 155094, 155095, 155096, 155097, 155098.

Jaculus blanfordi blanfordi (N = 50)

AMNH 212114, 212115, 244426; FMNH 103810, 103811, 103813, 103814, 103815, 103816, 103817, 103818, 103819, 103820, 103821, 103822, 103824, 103825, 103826, 103827, 103828, 103829, 103830, 103831, 112335, 112336, 112337, 112338, 112341; MVZ 192035, 198826; USNM 327067, 327068, 327069, 328531, 328532, 328535, 350747, 350748, 350749, 350750, 350751, 350752, 354836, 354837, 354838, 354839, 354840, 369524, 369525, 369526.

Jaculus hirtipes (N = 7)

FMNH 84751, 98205, 98206, 98208, 98210, 98211, 98212.

Jaculus jaculus (N = 34)

USNM 319782, 322762, 322763, 322765, 322768, 322769, 322770, 322771, 322772, 322773, 322781, 322784, 322785, 322786, 322787, 322788, 322789, 322790, 322791, 322792, 322799, 322800, 322801, 322802, 322803, 322804, 322808, 322809, 322810, 322818, 322819, 322820, 322822, 322823.

Jaculus jaculus Egypt (N = 27)

FMNH 100881, 100882, 100900, 100901, 100908, 100909, 100910, 100915, 100916, 100917, 101501, 101502, 68281, 74810, 77443, 77450, 77454, 77459, 78597, 79320, 84651, 84652, 89202; MVZ 107727, 34198, 34199, 34200.

Jaculus loftusi (N = 2)

FMNH 178899, 178900.

Jaculus orientalis gerboa (N = 57)

FMNH 100824, 100825, 100826, 100845, 100848, 100856, 74802, 74804, 77469, 77474, 77476, 78598, 78599, 79999, 80001, 82277, 82280, 84766, 84771, 84776, 84778, 84779, 84780, 84783, 84784, 84786, 84787; MVZ 32810; USNM 302276, 302277, 302278, 302279, 302280, 302281, 302282, 302289, 302290, 317069, 317072, 317074, 317075, 317077, 317083, 342042, 342043, 342044, 342046, 342048, 342049, 342054, 342137, 342138, 342139, 342140, 342141, 342142, 342143.

Jaculus orientalis mauritanicus (N = 7)

FMNH 65840; USNM 475856, 475857, 475888, 475980, 475982, 475983.

Stylodipus andrewsi (N = 18)

AMNH 58546, 58548, 58550, 58551, 58552, 58600, 58624, 58638, 58639, 58648, 58865, 58866, 84133; FMNH 30305, 30306, 30307, 30308, 30309.

References

Adams DC, Collyer ML, Kaliontzopoulou A, 2020. *Geomorph: Geometric Morphometric Analyses of 2D/3D Landmark Data*. https://cran.r-project.org/package=geomorph

Alhajeri BH, 2019. Cranial variation in geographically widespread dwarf gerbil *Gerbillus nanus* (Gerbillinae, Rodentia) populations: Isolation by distance versus adaptation to local environments. *J Zool Syst Evol Res* **57**:191–203.

Alhajeri BH, 2021a. A geometric morphometric analysis of geographic mandibular variation in the dwarf gerbil *Gerbillus nanus* (Gerbillinae, Rodentia). *J Mamm Evol* **28**:469–480.

Alhajeri BH, 2021b. Cranial variation in allactagine jerboas (Allactaginae, Dipodidae, Rodentia): A geometric morphometric study. *Zool Res* **42**:182–194.

Alhajeri BH, 2021c. A morphometric comparison of the cranial shapes of Asian dwarf hamsters (*Phodopus*, Cricetinae, Rodentia). *Zool Anz* **292**:184–196.

Alhajeri BH, 2022a. *Desmodilliscus braueri* crania compared to *Pachyuromys duprasi* (Desmodilliscini, Gerbillinae, Rodentia). *Mammalia* **86**:77–87.

Alhajeri BH, 2022b. Geometric differences between the crania of Australian hopping mice (*Notomys*, Murinae, Rodentia). *Aust Mammal* **44**:24–38.

Alhajeri BH, Fourcade Y, Upham NS, Alhaddad H, 2020a. A global test of Allen's rule in rodents. *Glob Ecol Biogeogr* **29**:2248–2260.

Alhajeri BH, Porto Lm V, Maestri R, 2020b. Habitat productivity is a poor predictor of body size in rodents. *Curr Zool* **66**:135–143.

Allen GM, 1925. Jerboas from Mongolia. *Am Museum Novit* **161**:1–6.

Ben Faleh A, Allaya H, Shahin AAB, 2016. Geographic patterns of genetic variation in the greater Egyptian jerboa *Jaculus orientalis* (Dipodidae, Rodentia) from Tunisia. *Biochem Syst Ecol* **68**:15–22.

Ben Faleh A, Cornette R, Annabi A, Said K, Denys C, 2013. Patterns of size and shape skull variability in Tunisian populations of *Jaculus jaculus* (Rodentia: Dipodidae). *Acta Zool Bulg* **65**:217–223.

Ben Faleh A, Cosson JF, Tatard C, Othmen AB, Said K et al., 2010. Are there two cryptic species of the lesser Jerboa *Jaculus jaculus* (Rodentia: Dipodidae) in Tunisia? Evidence from molecular, morphometric, and cytogenetic data. *Biol J Linn Soc* **99**:673–686.

Ben Faleh A, Granjon L, Tatard C, Boratyński Z, Cosson JF et al., 2012. Phylogeography of two cryptic species of African desert jerboas (Dipodidae: *Jaculus*). *Biol J Linn Soc* **107**:27–38.

Beolchini F, Corti M, 2004. The taxonomy of the genus *Tachyoryctes*: A geometric morphometric approach. *Ital J Zool* **71**:35–43.

Bergmann C, 1847. Über die Verhältnisse der Wärmeökonomie der Thiere zu ihrer Grösse. *Göttinger Stud* **3**:595–708.

Berman SL, 1985. Convergent evolution in the hindlimb of bipedal rodents. *J Zool Syst Evol Res* **23**:59–77.

Boratyński Z, Brito JC, Campos JC, Karala M, Mappes T, 2014. Large spatial scale of the phenotype-environment color matching in two cryptic species of African desert jerboas (Dipodidae: Jaculus). *PLoS One* **9**:e943421–e943429.

Cardini A, 2019. Craniofacial allometry is a rule in evolutionary radiations of placentals. *Evol Biol* **46**:239–248.

Cardini A, Polly PD, 2013. Larger mammals have longer faces because of size-related constraints on skull form. *Nat Commun* **4**:2458.

Cardini A, Polly D, Dawson R, Milne N, 2015. Why the long face? Kangaroos and wallabies follow the same 'rule' of cranial evolutionary allometry (CREA) as placentals. *Evol Biol* **42**:169–176.

Cheng J, Ge D, Xia L, Wen Z, Zhang Q et al., 2018. Phylogeny and taxonomic reassessment of jerboa, Dipus (Rodentia, Dipodinae), in inland Asia. *Zool Scr* **47**:630–644.

Cheng J, Lv X, Xia L, Ge D, Zhang Q et al., 2019. Impact of orogeny and environmental change on genetic divergence and demographic history of *Dipus sagitta* (Dipodoidea, Dipodinae) since the Pliocene in Inland East Asia. *J Mamm Evol* **26**:253–266.

Collyer ML, Adams DC, 2018. RRPP: An *R* package for fitting linear models to high-dimensional data using residual randomization. *Methods Ecol Evol* **9**:1772–1779.

Corbet GB, 1978. *The Mammals of the Palaearctic Region: A Taxonomic Review*. London: British Museum (Natural History).
Drake AG, Klingenberg CP, 2008. The pace of morphological change: Historical transformation of skull shape in St Bernard dogs. *Proc Biol Sci* **275**:71–76.
Darvish J, Hosseini F, 2005. New species of three-toed jerboa *Jaculus thaleri* sp. nov (Dipodidae: Rodentia) from the deserts of Khorasan Province, Iran. *Iran J Anim Biosyst* **1**:21–27.
Google. 2020. Google Maps. Version 3.42. https://maps.google.com/
Gunz P, Mitteroecker P, Neubauer S, Weber GW, Bookstein FL, 2009. Principles for the virtual reconstruction of hominin crania. *J Hum Evol* **57**:48–62.
Happold DCD, 1967. Biology of the jerboa *Jaculus jaculus butleri* (Rodentia, Dipodidae) in the Sudan. *J Zool* **151**:257–275.
Hoath R, 2003. *A Field Guide to the Mammals of Egypt*. Cairo: The American University in Cairo Press.
Holden ME, Musser GG, 2005. Family dipodidae. In: Wilson DE, Reeder DM, editors. *Mammal Species of the World: A Taxonomic and Geographic Reference*. 3rd edn. Baltimore (MD): Johns Hopkins University Press, 871–893.
Hutchins M, Kleiman D, Geist V, McDade M, 2003. *Grzimek's Animal Life Encyclopedia. Vol 16, Mammals V*. 2nd edn. Farmington Hills (MI): Gale Group.
Kang Y, Su J, Yao B, Ji W, Hegab IM et al. 2020. Geometric morphometric analysis of the plateau zokor *Eospalax baileyi* revealed significant effects of environmental factors on skull variations. *Zoology* **140**:125779.
Kingdon J, Happold D, Butynski T, Hoffmann M, Happold M et al., 2013. *Mammals of Africa. Vol III. Rodents, Hares and Rabbits*. New York: Bloomsbury Publishing.
Lay DM, 1972. The anatomy, physiology, functional significance and evolution of specialized hearing organs of gerbilline rodents. *J Morphol* **138**:41–120.
Lebedev VS, Bannikova AA, Lu L, Snytnikov EA, Adiya Y et al., 2018. Phylogeographical study reveals high genetic diversity in a widespread desert rodent *Dipus sagitta* (Dipodidae: Rodentia). *Biol J Linn Soc* **123**:445–462.
Lebedev VS, Bannikova AA, Pagès M, Pisano J, Michaux JR et al., 2013. Molecular phylogeny and systematics of Dipodoidea: A test of morphology-based hypotheses. *Zool Scr* **42**:231–249.
Li Y, Li Y, Li H, Wang J, Rong X et al., 2020. *Niviventer confucianus sacer* (Rodentia, muridae) is a distinct species based on molecular, karyotyping, and morphological evidence. *Zookeys* **959**:137–159.
Marcy AE, Hadly EA, Sherratt E, Garland K, Weisbecker V, 2016. Getting a head in hard soils: Convergent skull evolution and divergent allometric patterns explain shape variation in a highly diverse genus of pocket gophers (*Thomomys*). *BMC Evol Biol* **16**:207.
Mares MA, 1976. Convergent evolution of desert rodents: Multivariate analysis and zoogeographic implications. *Paleobiology* **2**:39–63.
Mares MA, 1980. Convergent evolution among desert rodents: A global perspective. *Bull Carnegie Museum Nat Hist* **16**:1–51.
Marr MM, MacLeod N, 2019. Geographical variation in Eurasian red squirrel (*Sciurus vulgaris* L., 1758) mandibles and the issue of subspecies-level organization: A failure of history? *Biol J Linn Soc* **128**:337–359.
Martínez JJ, Sandoval ML, Carrizo LV, 2016. Taxonomic status of large- and middle-sized *Calomys* (Cricetidae: Sigmodontinae) from the southern Central Andes inferred through geometric morphometrics of the skull. *J Mammal* **97**:1589–1601.
Michaux J, Shenbrot G, 2017. Family Dipodidae (jerboas). In: Wilson DE, Lacher TE, Mittermeier RA editors. *Handbook of the Mammals of the World, Vol. 7, Rodents II*. Barcelona: Lynx Edicions, 1–20.
Nokelainen O, Sreelatha LB, Brito JC, Campos JC, Scott-Samuel NE et al. 2020. Camouflage in arid environments: The case of Sahara-Sahel desert rodents. *J Vertebr Biol* **69**:20007.1.
Nowak RM, Paradiso JL, 1983. *Walker's Mammals of the World*. Vol **II**. 4th edn. Baltimore (MD): The Johns Hopkins University Press.
Osborn DJ, Helmy I, 1980. The contemporary land mammals of Egypt (including Sinai). *Fieldiana Zool* **5**:1–579.
Paradis E, Schliep K, 2019. ape 5.0: An environment for modern phylogenetics and evolutionary analyses in *R*. *Bioinformatics* **35**:526–528.
Prado JR, Percequillo AR, Pirani RM, Thomaz AT, 2022. Phenotypic and genomic differences between biomes of the South America marsh rat *Holochilus brasiliensis*. *Biol J Linn Soc* **135**:98–116.
R Core Team, 2020. *R: A Language and Environment for Statistical Computing*. Vienna: R Foundation for Statistical Computing.
Ranck GL, 1968. The rodents of Libya: Taxonomy, ecology and zoogeographical relationships. Washington (DC): Smithsonian Institution Press.
Rohlf FJ, 2015. The tps series of software. *Hystrix* **26**:1–4.
Rohlf FJ, Slice D, 1990. Extensions of the Procrustes method for the optimal superimposition of landmarks. *Syst Biol* **39**:40–59.
Ronez C, Barbière F, Santis LD, Pardiñas UFJ, 2020. Third upper molar enlargement in sigmodontine rodents (Cricetidae): Morphological disparity and evolutionary convergence. *Mammalia* **84**:278–282.
Scarpitti EA, Calede JJM, 2022. Ecological correlates of the morphology of the auditory bulla in rodents: Application to the fossil record. *J Anat* **240**:647–668.
Schneider CA, Rasband WS, Eliceiri KW, 2012. NIH image to ImageJ: 25 years of image analysis. *Nat Methods* **9**:671–675.
Setzer HW, 1956. Mammals of the Anglo-Egyptian Sudan. *Proc U S Natl Museum* **106**:447–587.
Shenbrot G, 2013. Geographic range, morphometric variation and niche differentiation in greater Egyptian jerboa *Jaculus orientalis*. *Mammalia* **77**:317–328.
Shenbrot G, Bannikova A, Giraudoux P, Quéré JP, Raoul F et al., 2017. A new recent genus and species of three-toed jerboas (Rodentia: Dipodinae) from China: A living fossil? *J Zool Syst Evol Res* **55**:356–368.
Shenbrot G, Feldstein T, Meiri S, 2016. Are cryptic species of the lesser Egyptian jerboa *Jaculus jaculus* (Rodentia, Dipodidae), really cryptic? Re-evaluation of their taxonomic status with new data from Israel and Sinai. *J Zool Syst Evol Res* **54**:148–159.
Shenbrot GI, Krasnov BR, Rogovin KA, 1999. *Spatial Ecology of Desert Rodent Communities*. Berlin, Heidelberg: Springer-Verlag.
Shenbrot GI, Sokolov VE, Heptner VG, Kovalskaya YM, 2008. *Jerboas: Mammals of Russia and Adjacent Regions*. Enfield: CRC Press.
South A, 2017. *rnaturalearth: World Map Data from Natural Earth*.
Sowerby A de C, 1920. XXXVII.—a new three-toed jerboa from China. *Ann Mag Nat Hist* **5**:279–281.
Tabatabaei YF, Alhajeri BH, 2018. Sexual dimorphism, allometry, and interspecific variation in the cranial morphology of seven *Meriones* species (Gerbillinae, Rodentia). *Hystrix* **29**:162–167.
Tavares WC, Vozniak JH, Pessôa LM, 2020. Evolution of appendicular specializations for fossoriality in euryzygomatomyine spiny rats across different Brazilian biomes (Echimyidae, Hystricognathi, Rodentia). *J Mamm Evol* **27**:299–314.
Taylor MC, Travouillon KJ, Andrew ME, Fleming PA, Warburton NM, 2021. Keeping an ear out: Size relationship of the tympanic bullae and pinnae in bandicoots and bilbies (Marsupialia: Peramelemorphia). *Curr Zool* **68**:251–264.
Thomas O, 1908. XXXIV.—A new jerboa from China. *Ann Mag Nat Hist* **2**:307–308.
Webster DDB, Webster M, 1975. Auditory systems of Heteromyidae: Functional morphology and evolution of the middle ear. *J Morphol* **146**:343–376.
Wickham H, 2016. *ggplot2: Elegant Graphics for Data Analysis*. New York: Springer-Verlag New York.
Wolak ME, Fairbairn DJ, Paulsen YR, 2012. Guidelines for estimating repeatability. *Methods Ecol Evol* **3**:129–137.
Zelditch ML, Swiderski DL, Sheets HD, 2012. *Geometric Morphometrics for Biologists: A Primer*. Cambridge (MA): Elsevier Science.